The Astrophysical Journal, 756:61 (11pp), 2012 September 1 doi:10.1088/0004-637X/756/1/61

ON THE EXISTENCE OF "RADIO THERMALLY ACTIVE" GALACTIC SUPERNOVA REMNANTS

D. Onić[1], D. Urošević[1,2], B. Arbutina[1], and D. Leahy[3]
[1] Department of Astronomy, Faculty of Mathematics, University of Belgrade, Serbia
[2] Isaac Newton Institute of Chile, Yugoslavia Branch
[3] Department of Physics and Astronomy, The University of Calgary, Canada
Received 2011 October 24; accepted 2012 July 4; published 2012 August 16

ABSTRACT

In this paper, we investigate the possibility of significant production of thermal bremsstrahlung radiation at radio continuum frequencies that could be linked to some Galactic supernova remnants (SNRs). The main targets for this investigation are SNRs expanding in high-density environments. There are several indicators of radio thermal bremsstrahlung radiation from SNRs, such as a flattening at higher frequencies and thermal absorption at lower frequencies intrinsic to an SNR. In this work, we discuss the radio continuum properties of three SNRs that are the best candidates for testing our hypothesis of significant thermal emission. In the case of SNRs IC 443 and 3C 391, thermal absorption has been previously detected. For IC 443, the contribution of thermal emission at 1 GHz, from our model fit is 3%–57%. It is similar to the estimate obtained from the thermal absorption properties (10%–40% at 1 GHz). In the case of the 3C 391 the conclusions are not so clear. The results from our model fit (thermal emission contribution of 10%–25% at 1 GHz) and results obtained from the low-frequency absorption (thermal contribution of 0.15%–7% at 1 GHz) do not overlap. For the SNR 3C 396 we suggest that if previously detected thermal absorption could be intrinsic to the SNR then the thermal emission (<47% at 1 GHz from our model fit) could be significant enough to shape the radio continuum spectrum at high frequencies. Polarization observations for these SNRs can constrain the strength of a thermal component. Reliable observations at low frequencies (<100 MHz) are needed as well as more data at high radio frequencies (>1 GHz), in order to make stronger conclusions about the existence of "radio thermally active" SNRs.

Key words: ISM: individual objects (3C 396, 3C 391, IC 443) – ISM: supernova remnants – radiation mechanisms: thermal – radio continuum: general

1. INTRODUCTION

The radio continuum emission from supernova remnants (SNRs) is believed to be mainly produced by the non-thermal synchrotron mechanism. The radio continuum spectrum is well fitted by a simple power law. On the other hand, the X-ray radiation from SNRs is produced by thermal bremsstrahlung and line radiation as well as by non-thermal synchrotron radiation (Reynolds 2008, and references therein). In this paper, we investigate the possibility of significant production of thermal bremsstrahlung radiation at radio frequencies from SNRs that fulfill certain conditions, as discussed below.

The approximate equation for the volume emissivity of thermal bremsstrahlung radiation $\varepsilon_\nu^{\mathrm{T}}$ for an optically thin ionized gas cloud at radio frequencies has the form

$$\varepsilon_\nu^{\mathrm{T}} = 6.8\times10^{-38}\, g_{ff}(\nu, T)\, n^2\, T^{-0.5}\ (\mathrm{erg\,cm^{-3}\,s^{-1}\,Hz^{-1}}), \quad (1)$$

where the number densities of electrons and ions are the same and given by n in $\mathrm{cm^{-3}}$, the temperature of the emitting region T is in K, and the thermally averaged Gaunt factor $g_{ff}(\nu, T)$ at radio frequencies is given by Gayet (1970) as

$$g_{ff}(\nu, T) \approx \begin{cases} 0.55\ln(4.96\times10^{-2}\nu^{-1}) + 0.82\ln T, \\ \quad 10^2\,\mathrm{K} < T < 9\times10^5\,\mathrm{K} \\ 0.55\ln(46.80\nu^{-1}) + 0.55\ln T, \\ \quad T \gtrsim 9\times10^5\,\mathrm{K} \end{cases}, \quad (2)$$

where frequency ν is in GHz.

From Equation (1) we see that if the number density increases, then the thermal volume emissivity increases (with the square of density). On the other hand, as temperature increases, the thermal volume emissivity decreases (approximately as $T^{-0.5}$). Figure 1 shows the thermal bremsstrahlung volume emissivity for a range of radio frequencies as a function of number density (1–$10^3\,\mathrm{cm^{-3}}$) and temperature (10^4–10^5 K). In the case of the post-Sedov–Taylor phase of SNR evolution, especially for those SNRs expanding in high-density environment, the thermal radio volume emissivity will increase with time as temperature decreases and density increases.

The SNR shock wave ionizes, heats, and compresses gas in the SNR environment. An SNR embedded in a high-density environment will become evolutionary old sooner than one which expands in the rarefied interstellar medium (ISM). The main hypothesis that we discuss in this paper is: if an SNR expands into a high-density ISM, e.g., a molecular cloud environment, significant thermal bremsstrahlung emission in the radio continuum from the SNR should be produced during its evolution.

In this paper, we analyze the possibility of significant thermal bremsstrahlung emission at radio frequencies from SNRs (Section 2). Furthermore, we propose methods for estimating the contribution of the thermal bremsstrahlung component in the total volume emissivity at 1 GHz and discuss the results for some possible "radio thermally active" Galactic SNRs (Sections 3 and 4). Due to their nature, we exclude from our analysis filled-center or Crab-like SNRs.

2. THEORETICAL OVERVIEW

2.1. Radio Continuum Spectra

The spectra of SNRs in radio continuum are usually represented by a power law (representing pure synchrotron radiation

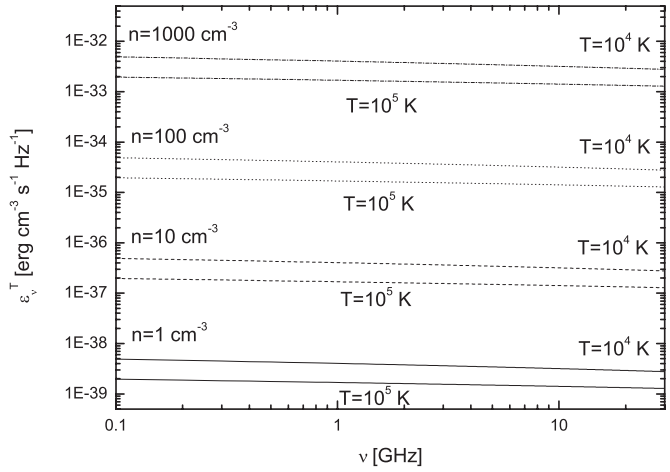

Figure 1. Thermal bremsstrahlung volume emissivity as a function of radio frequency for different number densities and temperatures.

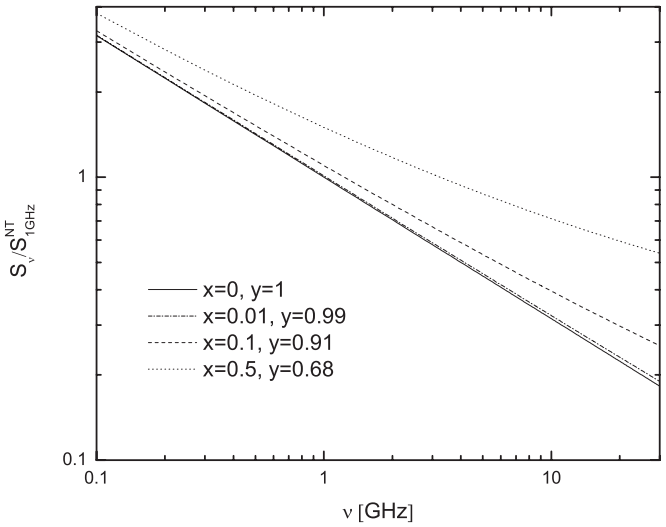

Figure 2. Curvature in an SNR radio spectrum due to existence of thermal bremsstrahlung emission in the case of the synchrotron spectral index of 0.5 and different values of x.

from the SNR shell). For frequency in units of GHz, the flux density can be represented by the following expression:

$$S_\nu = S_{1\,\mathrm{GHz}} \cdot \nu^{-\alpha}\ (\mathrm{Jy}), \tag{3}$$

where $S_{1\,\mathrm{GHz}}$ is the spatially integrated flux density at 1 GHz, and α is the radio spectral index.

Observed radio spectral indices vary from around 0.3 to 0.8 for Galactic SNRs (see Green 2009). Test-particle diffusive shock acceleration (DSA) theory predicts that for strong shocks, the radio spectral index is approximately 0.5. In the case of shocks with Mach number less than around 10, steeper spectra are expected; on the other hand, few SNRs would be expected to have such weak shocks (Reynolds 2011). Steeper radio spectra may also be explained by nonlinear effects. An important prediction of the modified shock explanation, where the reaction effects of cosmic-ray (CR) particle pressure is taken into account, is that the spectrum should flatten at higher energies so that a "concave up" spectrum is formed (see Reynolds 2008, and references therein). In the case of young SNRs, where the acceleration process is efficient, there is some evidence for spectral curvature, although better measurements with smaller errors are needed (Allen et al. 2008; Reynolds & Ellison 1992). Bell et al. (2011) noted that the total steepening may be a cumulative effect of nonlinear and oblique-shock steepening in the case of young SNRs. On the other hand, observations over a very broad range of radio frequencies reveal a curvature in the spectra of some evolutionary older Galactic SNRs (Urošević & Pannuti 2005; Tian & Leahy 2005; Leahy & Tian 2006; Urošević et al. 2007; Onić & Urošević 2008).

When the spectral index is changing with frequency there is a possibility that two different mechanisms are producing the radio emission. The presence of thermal bremsstrahlung radiation would change the shape of the radio spectrum to be "concave up," especially in the case of SNRs evolving in a dense environment (evolutionary old SNRs).

If we take the approximative formula for the Gaunt factor at radio frequencies from Cooray & Furlanetto (2004 and references therein): $g_{ff}(\nu, T) \approx 11.96 T^{0.15}\nu^{-0.1}$ we can write for the sum of thermal bremsstrahlung ($\varepsilon_\nu^{\mathrm{T}}$) and non-thermal synchrotron ($\varepsilon_\nu^{\mathrm{NT}}$) emissivities:

$$\varepsilon_\nu = \varepsilon_\nu^{\mathrm{NT}} + \varepsilon_\nu^{\mathrm{T}} = \varepsilon_{1\,\mathrm{GHz}}^{\mathrm{NT}}\nu^{-\alpha} + \varepsilon_{1\,\mathrm{GHz}}^{\mathrm{T}}\nu^{-0.1}, \tag{4}$$

where frequency ν is in GHz. For optically thin emission we can write a similar formula for the total flux density:

$$S_\nu = S_\nu^{\mathrm{NT}} + S_\nu^{\mathrm{T}} = S_{1\,\mathrm{GHz}}^{\mathrm{NT}}\nu^{-\alpha}(1 + x\nu^{\alpha-0.1}), \tag{5}$$

where $x = S_{1\,\mathrm{GHz}}^{\mathrm{T}}/S_{1\,\mathrm{GHz}}^{\mathrm{NT}}$ is the ratio of the thermal and non-thermal flux densities at 1 GHz.

As radio frequency increases, both thermal and non-thermal emissions are decreasing. The non-thermal spectrum is steeper than the thermal bremsstrahlung spectrum. If significant thermal radiation is emitted then the slope of the radio spectrum will change (concave up spectrum) at higher radio frequencies (>1 GHz). This is clearly seen in Figure 2, which illustrates the case for a synchrotron spectral index of 0.5 and different values of x. Another phenomenon, seen in Figure 2, is that the value of the power-law index obtained by fitting the total spectrum will have a lower value than the intrinsic synchrotron spectral index. The relative change in the radio spectral index is $y = \alpha_{\mathrm{total}}/\alpha_{\mathrm{synch.}}$, where α_{total} represents the radio spectral index estimated from the power-law fit and $\alpha_{\mathrm{synch.}}$ represents the synchrotron spectral index.

It must be noted that there is a possibility that different areas of the SNR have different non-thermal spectra (for example, because of different evolutionary stages). If the spectral indices are not changing over the SNR and spectral flattening exists at higher frequencies, that could be indication of significant thermal emission from the SNR (assuming that there is no contamination by overlapping thermal sources). On the other hand, radio spectral index variations, detected in some SNRs and associated with parts of the SNR where density is higher than average (inhomogeneous medium with high-density cloudlets, high-density gradients due to vicinity of the molecular cloud) could be explained by intrinsic SNR thermal emission. However, the non-association of high linear polarization percentages with those regions is essential for validation of this claim.

There is also a significant number of Galactic SNRs with $\alpha < 0.5$. Contamination with flat spectrum thermal emission may be responsible for the lower spectral index values. It is also possible, in the case of such a flatter spectra, that second-order Fermi (or stochastic) acceleration plays a major role (Reynolds 2008 and references therein). Schlickeiser & Fürst (1989) concluded that the observed dispersion in spectral

index values below $\alpha = 0.5$ is attributed to a distribution of low plasma β values ($\beta \simeq 0.05$) in different remnants ($\beta = 8\pi P/B^2 \propto (V_{\rm sound}/V_A)^2$, where P is the gas pressure, B is the magnetic induction, $V_{\rm sound}$ is the adiabatic sound speed, and V_A is the Alfvén speed). Ostrowski (1999) pointed out that shock waves with Alfvén speed non-negligible in comparison to the shock velocity are responsible for generation of the flat particle distribution. The corresponding analysis was applied to the SNRs W44 and IC 443. The flatter spectra may also be due to compression ratios greater than four at radiative shocks (Bell et al. 2011). It must be noted that there are no predictions of curved—"concave up"—radio spectra in the cases of the mentioned explanations of the flat radio spectra seen in some SNRs.

One of the characteristics of the so-called mixed-morphology (thermal composite) SNRs[4] (Rho & Petre 1998; Vink 2012) is that they usually have $\alpha < 0.5$ based on a pure synchrotron fit (Green 2009). On the other hand, they are known to expand in a high-density environment (many of them interacting with molecular clouds) and are mainly evolutionary old. Tilley et al. (2006) emphasized that SNRs expanding into denser ISM might spend a significant fraction of their observable lives as mixed-morphology remnants. That marks mixed-morphology remnants as the best candidates for the investigation of the possible production of significant thermal bremsstrahlung radiation at radio frequencies. On the other hand, Uchiyama et al. (2010) proposed that the radio emission may be additionally enhanced by the presence of secondary electrons/positrons, i.e., the products left over from the decay of charged pions, created due to CR nuclei colliding with the background plasma. The presence of secondary electrons/positrons may also explain the flat spectral radio indices of some mixed-morphology SNRs (Uchiyama et al. 2010). This model, on the other hand, does not produce a "concave up" radio spectrum.

2.2. Thermal Bremsstrahlung Radiation in the Radio Continuum

Here, we investigate the hypothesis that in the case of SNRs in the late and post-Sedov–Taylor phases it is likely that the reason for a curved (concave up) radio continuum spectrum is a significant presence of thermal bremsstrahlung radiation. We discuss a situation in which the ensemble of thermal electrons, linked to an SNR, could significantly radiate at radio frequencies.

First, we consider the case where DSA is the only process of acceleration. The fraction of protons and electrons in a gas that are pre-accelerated to an energy at which they are injected into the acceleration mechanism is around 10^{-3} (Bell 1978a, 1978b; Berezhko & Völk 2004). This leaves the possibility of the existence of a great pool of thermal electrons that can radiate, so we can talk about two populations of electrons: thermal and relativistic. The number of relativistic electrons is always negligible compared to the thermal electrons, but thermal electrons can have temperatures of 10^6 K. Vink et al. (2010) and Drury et al. (2009) pointed out that the post-shock (downstream) gas temperature could be significantly reduced by acceleration. For young SNRs and Mach numbers $M > 75$, the downstream temperature is at least 80 times the upstream temperature (Vink et al. 2010). One of the consequences of efficient CR acceleration is that the highest energy CRs may escape far upstream (i.e., into the unshocked medium) forming a CR shock precursor. Nonlinear CR acceleration leads to lower plasma temperatures, in the most extreme cases perhaps even quenching thermal X-ray emission (Vink 2012 and references therein). Directly upstream of the shock, the CRs provide a non-negligible pressure, which pre-compresses and pre-heats the plasma (Vink 2012). The most important phases for particle acceleration are the transition into the Sedov–Taylor phase and the early Sedov–Taylor phase (Reynolds 2008). The radio synchrotron luminosity increases with time in the free expansion phase, achieves its peak value at the very beginning of the Sedov phase, and then again decreases with time (Berezhko & Völk 2004). We suggest that, even when DSA is not too weak, there can be significant thermal bremsstrahlung radiation at radio continuum frequencies from SNRs expanding in a high-density environment with lower temperatures.

It is known that in the case of radiative J shocks, a photoionized precursor is formed. Half of the photons produced in the cooling zone downstream to the shock pass upstream, where they are absorbed by the upstream gas. The ambient material becomes ionized so if its density is high, preserving the optically thin medium, there is the possibility of significant thermal bremsstrahlung radiation at radio continuum frequencies. As Brogan et al. (2005) concluded in the case of free–free absorption observed toward SNR 3C 391, ionized gas can be produced when the SNR blast wave encounters a nearby molecular cloud with sufficient speed to dissociate and ionize the gas.

Pynzar' & Shishiv (2007 and references therein) analyzed thermal emission and absorption in and near directions toward SNRs and used it to estimate the distribution of ionized gas surrounding SNRs of Type II supernovae. They concluded that the kinetic energy of a Type II supernova envelope is transformed into radiation at an early stage in the evolution of the object, leading to the formation of an H II region in the vicinity of the SNR or young pulsar. This could mean that the thermal radio emission is inherent to SNRs.

In the case of older SNRs, it is not yet known whether the mechanism for producing relativistic electrons is local acceleration at a shock front or compression of the existing population of Galactic background relativistic electrons (Leahy 2006 and references therein). A variable magnetic field strength is expected in older SNRs. The compression ratio in radiative shocks can be very large, resulting in a stronger and more strongly variable magnetic field. Analyzing the spectral index variation in the case of SNR HB21, Leahy (2006) pointed out that the variable magnetic field causes the observed frequency range to correspond to variable energy range in the electron spectrum, so that either positive or negative curvature in the electron spectrum results in variable observed spectral index in a fixed radio frequency range. Leahy & Roger (1998) analyzed radio spectral index variations for the Cygnus Loop and pointed out that a radio spectrum with concave up (positive) curvature can be produced by adding two different emission spectra along the same line of sight or within the same emitting volume (possibly due to two different electron populations).

2.3. The Low-frequency Turnovers

Detected concave down (negative) spectral curvature at low frequencies is believed to be due to absorption by a thermal plasma, although the possibility of synchrotron self-absorption is not ruled out. The low-frequency turnovers have been usually attributed to free–free absorption in ionized thermal gas along the line of sight to the SNR, although it could be also directly

[4] The mixed-morphology SNRs are with bright interiors in X-rays and bright rims in radio.

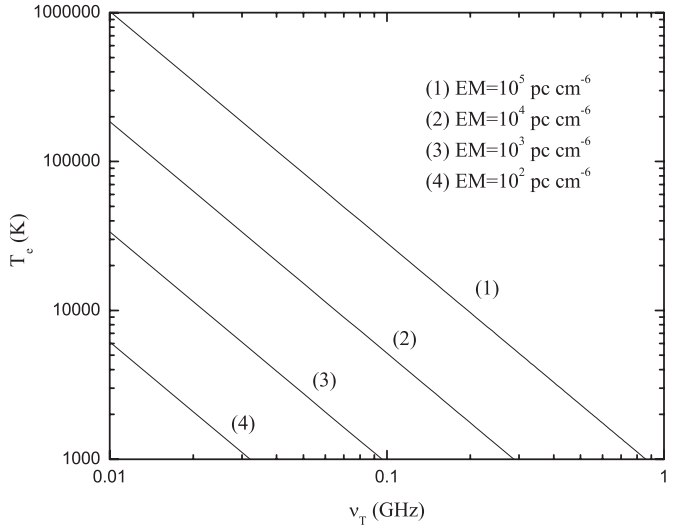

Figure 3. Thermal cutoff frequency $\nu_{\rm T}$ dependence on electron temperature T_e and emission measure EM.

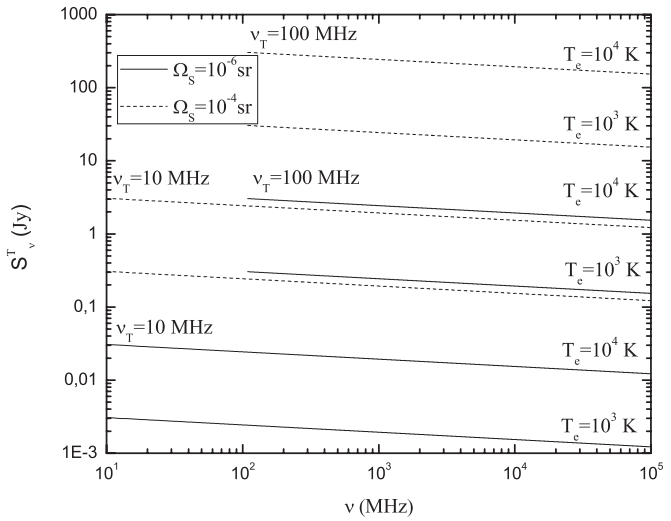

Figure 4. Thermal flux density vs. frequency for different values of turnover frequency $\nu_{\rm T}$, electron temperature T_e, and source solid angle Ω_S based on Equations (8) and (9).

linked to some SNRs (e.g., 3C 391, IC 443; see Brogan et al. 2005 and Castelletti et al. 2011). Thermal absorption, at low frequencies, inherent to an SNR, could be a sign of possible thermal emission at high frequencies.

Since thermal absorption could be present at lower frequencies, we estimate the thermal cutoff frequency ($\nu_{\rm T}$) dependence on electron temperature (T_e (K)) and emission measure (EM (cm^{-6} pc)) and present it in Figure 3. We can write (Altenhoff et al. 1960)

$$\nu_{\rm T} \approx 0.3045 T_e^{-0.643} {\rm EM}^{0.476}\ ({\rm GHz}), \tag{6}$$

where

$$ {\rm EM} = \int_0^s n_e^2 ds. \tag{7}$$

For example, for IC 443, we calculated $\nu_{\rm T} \approx$ (30–50) MHz for an assumed T_e = (8000–12,000) K and EM = (2.8–5) $\times$ 10^3 cm^{-6} pc (eastern rim; Castelletti et al. 2011) and 3C 391 $\nu_{\rm T} \approx$ (40–150) MHz for an assumed T_e = (1000–3000) K and EM = (0.6–2.5) $\times$ 10^3 cm^{-6} pc (Brogan et al. 2005). In the case of 3C 391, Anantharamaiah (1985) suggested the upper limits of EM = 2500 cm^{-6} pc and T_e = 8000 K.

If the low-frequency turnover due to thermal absorption is inherent to an SNR, we can calculate the flux density at the turnover frequency ν_T from the Rayleigh–Jeans formula:

$$S_{\nu_T} = \frac{2kT_e\Omega_S\nu_T^2}{c^2} \tag{8}$$

and then calculate the flux density at any higher frequency from

$$S_\nu = S_{\nu_T}\left(\frac{\nu}{\nu_T}\right)^{-0.1}, \tag{9}$$

where k is the Boltzmann constant, c is the speed of light, Ω_S is the source solid angle, and T_e is the electron temperature. If there is an estimate of T_e, we can compare the flux density at 1 GHz obtained from the low-frequency absorption for a given SNR with the directly measured integrated flux density. In Figure 4, the thermal flux density versus frequency is plotted, for different values of $\nu_{\rm T}$, T_e, and Ω_S based on Equations (8) and (9). Solid lines are for $\Omega_S = 10^{-6}$ sr, while dotted lines are for $\Omega_S = 10^{-4}$ sr. Low-frequency free–free thermal absorption may provide an important complementary tracer of fast ionizing SNR/molecular cloud shocks (for details, see Brogan et al. 2005) as well as of thermal bremsstrahlung emission.

2.4. SNR Dynamical Evolution and Thermal Bremsstrahlung Emission

In the Sedov–Taylor phase, the downstream temperature T (where the radiation is generated) and the shock radius can be expressed by (Yamauchi et al. 1999)

$$T = 2.07 \times 10^{11}\left(\frac{E_{51}}{n_a}\right)^{0.4} t^{-1.2}\ ({\rm K}), \tag{10}$$

$$R_S = 0.315\left(\frac{E_{51}}{n_a}\right)^{0.2} t^{0.4}\ ({\rm pc}), \tag{11}$$

where the age is expressed in years and the initial explosion energy is E: $E_{51} = E\,({\rm erg})/10^{51}$. Petruk (2005) noted that the transition time $t_{\rm tr}$ is defined as the end of the energy conserving stage and the beginning of the radiative stage (so the Sedov–Taylor approximation is valid before $t_{\rm tr}$). The shell formation time $t_{\rm sf}$ marks the time when the so-called pressure-driven snowplow phase defined by McKee & Ostriker (1977) starts, in which interior hot gas pushes the cold dense shell (the "deceleration parameter," defined as $m = d\log R_S/d\log t$, is 2/7). The structure of the flow is re-structurized and a thin shell is formed during the so-called transition sub-phase given by the time interval ($t_{\rm tr}$, $t_{\rm sf}$). Petruk (2005) gave equations for $t_{\rm tr}$ and $t_{\rm sf}$:

$$t_{\rm tr} = 2.84 \times 10^4 E_{51}^{4/17} n_a^{-9/17}\ ({\rm yr}) \tag{12}$$

$$t_{\rm sf} = 5.20 \times 10^4 E_{51}^{4/17} n_a^{-9/17}\ ({\rm yr}). \tag{13}$$

The transition time $t_{\rm tr}$, the shell formation time $t_{\rm sf}$, the shock radius $R_{\rm tr}$, the temperature $T_{\rm tr}$, and the shock velocity $V_{\rm tr}$ for SNRs which expand in environments with different ambient number densities n_a, with $E_{51} = 1$, are given in Table 1. It is clearly seen that SNRs which expand in higher density environments are smaller and younger when they leave the energy conserving phase. SNRs which expand in a high-density

Table 1
Transition and Shell Formation Time as well as Radius, Temperature, and Shock Velocity at the Transition Time for SNRs Expanding in the Environments with Different Ambient Densities with $E_{51} = 1$

n_a (cm^{-3})	t_{tr} (yr)	t_{sf} (yr)	R_{tr} (pc)	T_{tr} (K)	V_{tr} ($km\,s^{-1}$)
0.01	3.25×10^5	5.95×10^5	126.56	3.21×10^5	152
0.1	9.61×10^4	1.76×10^5	49.03	5.53×10^5	199
1	2.84×10^4	5.20×10^4	19.00	9.5×10^5	261
10	8.39×10^3	1.54×10^4	7.36	1.63×10^6	342
100	2.48×10^3	4.54×10^3	2.85	2.81×10^6	449
1000	7.33×10^2	1.34×10^3	1.11	4.83×10^6	584

environment evolve (and leave the Sedov–Tayler phase) faster than those in a low-density environment. The approximate analytical solutions are not adequate for the post-Sedov–Tayler phases, so that numerical simulations are needed.

Weakening of the SNR shock in the post-Sedov–Taylor phase lowers the temperature of the shell as well as of the thermal X-ray emitting region (therefore reducing the extent of that region). The Sedov–Taylor phase ends when the shock is slow enough (usually $\sim$200 km s^{-1}) that significant radiative cooling can take place and the adiabatic approximation breaks down. Significant radio thermal bremsstrahlung emission could arise from the cooled thermal X-ray electrons. On the other hand, local regions of the blast wave may become radiative sooner where the ambient density is much higher than average, though the bulk evolution is still adiabatic (Reynolds 2008). Different parts of an SNR may be in different phases. SNRs could have both radiative and non-radiative shocks. This could also give rise to significant radio thermal bremsstrahlung emission from the parts of an SNR in the radiative phase. For example, earlier in its evolution, the Cygnus Loop must have expanded rapidly within the tenuous medium inside the wind-blown bubble. Vink (2012) pointed out that, currently, the largest part of the shock of Cygnus Loop is interacting with a dense shell swept up by the progenitor's wind. Another example is RCW 86 which also shows a mixture of radiative and non-radiative shocks (Vink 2012).

As already mentioned, mixed-morphology SNRs are characterized by centrally peaked thermal X-ray emission with shell-like radio morphology. Their interiors are more or less homogeneous in temperature and, because of pressure equilibrium, also reasonably homogeneous in density (Vink 2012). The Sedov–Taylor model is not applicable for mixed-morphology SNRs and their observational properties differ from those expected for an evolved SNR in a homogeneous ISM (Yamaguchi et al. 2012). More complex models are needed to explain the mechanism responsible for the observed characteristics of mixed-morphology SNRs. Radiative recombination continuum (RRC) was recently discovered in their X-ray spectra (Yamaguchi et al. 2012 and references therein). The presence of strong RRC is evidence that the plasma is recombining. Most of the mixed-morphology SNRs appear to be in the radiative phases of their evolution, with shock velocities less than 200 km s^{-1} (Vink 2012), which results in cool, X-ray dim, but optical/UV bright regions immediately behind the shock front. It is likely that a significant pool of cooled thermal electrons exist. Vink (2012) noted that the high density in the interior of mixed-morphology SNRs is a direct consequence of the high ISM density and thermal conduction, which results in a more uniform interior density with medium hot temperatures, rather than very high temperatures for the case of very low interior densities.

2.5. The Thermal Radio Luminosity and Possibility of Ambient Density Estimation from Radio Continuum Emission

Luminosity and flux density are related by

$$L_\nu = 4\pi d^2 S_\nu, \tag{14}$$

where d is the distance to an SNR. The thermal luminosity, on the other hand, can be expressed as

$$L_\nu^{\mathrm{T}} \approx \varepsilon_\nu^{\mathrm{T}} V_{\mathrm{shell}} = 2 \times 10^{18} g_{ff}(\nu, T) n^2 T^{-0.5} \frac{4\pi}{3} R_S^3 f, \tag{15}$$

where L_ν^{T} is in (erg s^{-1} Hz^{-1}), n(cm^{-3}), T(K), shock radius R_S(pc), and f is the volume filling factor.

In the Sedov–Taylor phase, the compression ratio is nearly equal to 4 so we can approximately write $n \approx 4n_a$, where n_a is the average ambient number density ($\rho_{\mathrm{ISM}} = n_a \mu m_{\mathrm{H}}$, where ρ_{ISM} is the ambient density, μ is the mean molecular weight and $m_{\mathrm{H}} = N_A^{-1}$, where N_A is Avogadro's number). We can also roughly assume for the volume filling factor of the shell: $f \approx 0.25$. For the Sedov–Taylor phase, the thin shell approximation is only moderately accurate (Bandiera & Petruk 2004).

For a standard value of $E_{51} = 1$ using Equations (2) and (15), in the case of the Sedov–Taylor phase (using Equations (10) and (11)), we can write

$$L_{1\,\mathrm{GHz}}^{\mathrm{T}} \approx \begin{cases} 1.66 \times 10^{15} f n_a^{2.5} R_S^{4.5} (16.99 - 0.82 \ln n_a - 2.48 \ln R_S), \\ \quad T < 9 \times 10^5\ \mathrm{K} \\ 1.66 \times 10^{15} f n_a^{2.5} R_S^{4.5} (14.54 - 0.55 \ln n_a - 1.65 \ln R_S), \\ \quad T \gtrsim 9 \times 10^5\ \mathrm{K} \end{cases}, \tag{16}$$

From Truelove & McKee (1999) we can estimate the shock radius at the beginning of the energy conserving phase (approximately for the case of uniform ambient medium and ejecta):

$$R_{\mathrm{ST}} \approx 2.23 \left(\frac{M_{\mathrm{ej}}}{M_\odot} \right)^{1/3} n_a^{-1/3}\ (\mathrm{pc}). \tag{17}$$

An $L_{1\,\mathrm{GHz}}^{\mathrm{T}}$–$R_S$ plot can also give us an insight into the type of the SNR phase if we could calculate the $L_{1\,\mathrm{GHz}}^{\mathrm{T}}$ from the observations and our model fit (see Figure 5).

It is worth comparing Figure 5 with a similar graph for pure synchrotron emission (see Section 5 and Figure 4 in Berezhko & Völk 2004). In the classical Sedov–Taylor phase, the luminosity of thermal radiation is $\approx$4 orders of magnitudes less than synchrotron radiation so it does not significantly contribute to the overall radio continuum spectrum. We used $f = 0.25$ so that different volume filling factor values could change the results by factors of a few. The endpoints of the thermal luminosity lines for the Sedov–Taylor phase (see Figure 5) represent the moment when an SNR reaches R_{tr} (see Table 1). The dashed line in Figure 5 connects points that represent the beginning of the Sedov–Taylor phase (Equation (17)) if $M_{\mathrm{ej}} = 10\,M_\odot$. This contrasts with $M_{\mathrm{ej}} = 1.4\,M_\odot$ assumed for the shown starting points (Truelove & McKee 1999). During the energy conserving phase and at the beginning of the radiative phases the contribution of thermal radio emission is negligible. We can see from Table 1 that the temperature at the end of the Sedov–Taylor phase is around 10^5–10^6 K and it is

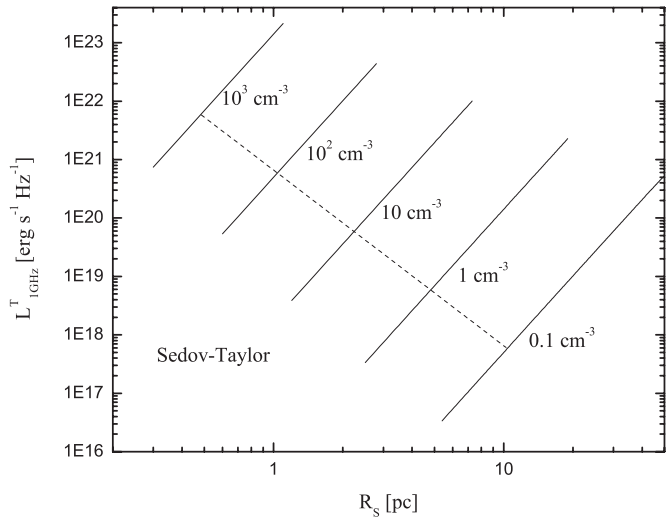

Figure 5. $L^{T}_{1\,GHz}$ vs. R_S in the case of a Sedov–Taylor SNR for different values of ambient density. The endpoints of the thermal luminosity lines for pure Sedov–Taylor phase represent the moment when an SNR reaches R_{tr}. The dashed line connects points that represent the beginning of the Sedov–Taylor phase if $M_{ej} = 10\,M_\odot$ in contrast to the $M_{ej} = 1.4\,M_\odot$ assumed for the shown starting points.

nearly independent of explosion energy and ambient density. To decrease this temperature significantly either the explosion energy or the ambient density must be unrealistically low. If we can detect significant thermal X-ray emission the temperature has to be of the order of 10^6 K or at least a few 10^5 K and then the radio bremsstrahlung emissivity would be too low.

As we already pointed out, the evolution of an SNR could be more complicated than that given by the classical Sedov–Taylor model. In the case when an SNR expands in an inhomogeneous medium, local regions of the blast wave may become radiative sooner where the ambient density is much higher than average, though the bulk evolution is still governed by the Sedov–Taylor phase. The high-density regions of an SNR populated by cooled thermal X-ray electrons could account for significant radio thermal luminosity ($L^{T}_{\nu} \propto n^2$) that could be comparable with synchrotron emission. In the Sedov–Taylor phase L^{NT}_{ν} is approximately independent of the density (Berezhko & Völk 2004). At a given SNR diameter, all SNRs in the Sedov–Taylor phase should have roughly the same synchrotron spectral luminosity, with some spread due to explosion energy. On the other hand, SNRs in denser media reach the Sedov time (corresponding to their peak luminosity) when they still have relatively small diameters. Therefore, their peak spectral luminosity is brighter than that of SNRs in lower density media, and they continue to be more luminous through much of the Sedov–Taylor phase (Chomiuk & Wilcots 2009 and references therein). However, for radiative shocks, the shock compression factors are large, giving rise to strongly compressed magnetic fields, and enhanced CR electron densities, so the radio synchrotron emission could be also strongly enhanced (Vink 2012 and references therein). We emphasize the importance of the analysis of evolution (and radiation) of SNRs which include more complex models of SNR dynamics.

3. THE MODEL

In order to distinguish the contribution of thermal and non-thermal components in the total emission, the SNR radio integrated spectrum can be fitted by a sum of these two components (error-weighted least squares). For frequencies in GHz, the relation for the integrated flux density can be written as follows:

$$S_\nu = S^{NT}_{1\,GHz}\left(\nu^{-\alpha} + \frac{S^{T}_{1\,GHz}}{S^{NT}_{1\,GHz}}\,\nu^{-0.1}\right)\ (\mathrm{Jy}), \qquad (18)$$

where $S^{T}_{1\,GHz}$ and $S^{NT}_{1\,GHz}$ are flux densities corresponding to the thermal and non-thermal components, respectively. We used weighted (instrumental errors) nonlinear least squares for fitting.

The whole SNR is assumed to be optically thin at radio frequencies and the thermal emission has spectral index equal to 0.1. It is assumed that the synchrotron radiation is not absorbed or scattered by the thermal gas. Also, the radio spectral index is assumed to be constant in the SNR shell. The most important distinction between the presence of thermal emission or simply a particle acceleration model that produces a flat spectrum is the fact that the spectral index changes with frequency, a "concave up" spectrum is formed, because the low frequencies are dominated by steep spectrum synchrotron emission and the high frequencies by flat spectrum thermal emission. SNRs that do produce significant thermal emission are in a later evolutionary stage. As we have already mentioned, these SNRs can have different parts in different phases of evolution, with the possibility of producing synchrotron emission with different spectral indices in different areas. Quite naturally, the flatter spectrum would dominate the high-frequency part and the steeper spectrum the low-frequency regime. This is one of the major problems of our model. To avoid that problem, it has to be shown that the spectral index is not changing very much over the SNR. This is very difficult, in practice, with observations from various archives, observed at a wide frequency range, at various resolutions. On the other hand, as we already noted, radio spectral index variations, associated with parts of an SNR where the density is higher than average and for which linear polarization percentages are negligible, could be explained by intrinsic SNR thermal emission.

This model is valid in the approximation of constant density and temperature in the emitting shell. The model itself also assumes a simple sum of non-thermal and thermal components. We note that this model, in general, does not distinguish between intrinsic and foreground/background thermal emission.

In the case of SNR expansion in the vicinity of an H II region, the thermal emission from an SNR and adjacent H II region cannot be separated within our model. This is a serious problem especially since we are interested in the analysis of the integrated SNR spectrum. In the case when there is an overlapping H II region, it is very difficult to separate the thermal contribution from the H II region from the SNR's thermal emission. A visual inspection of radio maps should show whether an H II region overlaps with an SNR, so that it could be avoided. We treat such cases with caution, but point out that the existence of the contamination by an H II region emission does not rule out thermal bremsstrahlung emission from the SNR, it can just mask it.

Another important problem is that our model is sensitive to small changes in the observations. Deriving accurate integrated flux densities is in fact difficult. It depends on details of individual observations (e.g., definition of the area that was integrated or usage of a simplistic Gaussian model; background emission correction; whether the observations are on the same flux density scale, and whether flux densities are comparable, i.e., integrated from the same regions). There is also a problem with total flux densities taken from the literature. Some of the authors subtract

Table 2
Fit Parameters for Our Model and a Purely Non-thermal Model for SNR IC 443

α	$S^{\rm NT}_{1\,\rm GHz}$ (Jy)	$\frac{S^{\rm T}_{1\,\rm GHz}}{S^{\rm NT}_{1\,\rm GHz}}$	χ^2/dof	Adj. R^2
0.82 ± 0.35	96.40 ± 40.50	0.68 ± 0.65	1.72	0.83
0.47 ± 0.06	165.40 ± 7.80	···	1.74	0.83

the contribution from point sources others do not. Some authors cannot even subtract them because the resolution of their maps is not good enough. That is in particular a problem at low frequencies. Since these point sources are usually extragalactic in origin they could—if not subtracted—steepen the total spectrum toward lower frequencies which would make it appear as if the spectrum is concave upward toward higher frequencies.

The small number of data points and the dispersion of the flux densities at the same frequencies make for uncertain fitting with our model. More data at radio frequencies higher than 1 GHz are necessary in order to make firmer conclusions about the significance of thermal emission.

Despite these drawbacks, this model can give us a rough insight into whether or not there might be a significant contribution of thermal bremsstrahlung component to the total volume emissivity at radio frequencies.

Possible thermal bremsstrahlung radiation at radio frequencies from SNRs was discussed by Urošević & Pannuti (2005). A similar model, but in the case of spiral galaxies, was introduced by Duric et al. (1988).

There are other important tracers of the thermal emission that could be used to support or dismiss the presence of thermal radio emission from SNRs. Linear polarization measurements give us lower limits for the non-thermal component of the radio emission. Detection in Hα (see Stupar & Parker 2011) as well as radio recombination lines implies that a significant amount of thermal electrons must be present. Weak radio recombination line emission has been observed toward several SNRs and it has remained unclear if this emission is in fact associated with SNRs or due to intervening sources such as extended H II envelopes along the line of sight (Hewitt & Yusef-Zadeh 2006).

4. ANALYSIS AND RESULTS

We have investigated the radio continuum spectra of the 24 known mixed-morphology SNRs (Vink 2012). We also investigated shell and composite SNRs known to expand in high-density environments with some of tracers of possible thermal emission: curved spectrum, thermal absorption at low frequencies intrinsic to an SNR, detection in radio recombination lines and Hα, spectral index variations. We used only flux densities with errors $\leqslant$20% from the literature and used only those flux densities that are on the scale of Baars et al. (1977). We did not analyze the SNRs with only four or less data points found.

In this work, we discuss the radio continuum properties of three SNRs that are the best candidates for testing our hypothesis of significant thermal emission.

4.1. IC 443 (G189.1+3.0) and 3C 391 (G31.9+0.0)

IC 443 and 3C 391 both expand in a high-density environment (and interact with molecular clouds) and exhibit thermal absorption at low frequencies which is linked to the SNRs (Brogan et al. 2005; Castelletti et al. 2011).

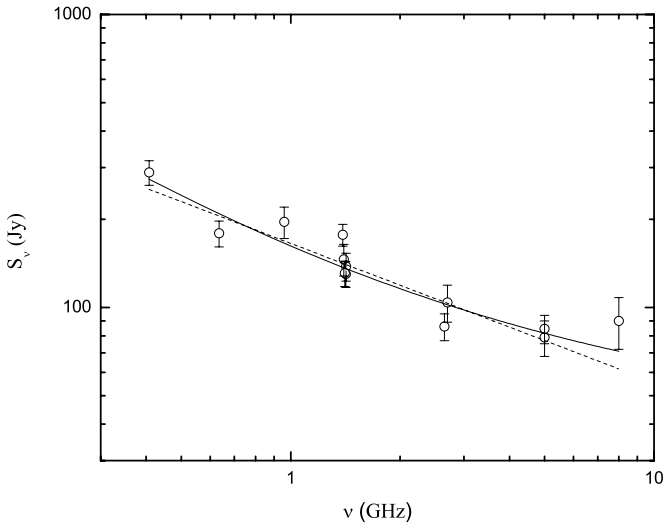

Figure 6. Integrated spectrum of SNR IC 443. The full line represents the least-squares fit by the non-thermal plus thermal model, while the dotted line represents the fit by the purely non-thermal model. Only data on the scale of Baars et al. (1977) were used.

4.1.1. IC 443

From our model fit to IC 443 (Table 2 and Figure 6), the contribution of thermal emission at 1 GHz is between 3% and 57% (the range of frequencies used here is from 408 MHz to 8 GHz). We used the data from Castelletti et al. (2011) and Gao et al. (2011). $\chi^2_{\rm red}$ represents the χ^2/dof, where dof is the degree of freedom. Adj. R^2 represents the fit quality.[5] If we add all the data from Table 2 of Castelletti et al. (2011) with errors less than 20%, excluding the point at 10 MHz (range of frequencies between 20 MHz and 8 GHz), from our model fit, we find that there is no significant thermal emission from IC 443. More data, especially between 10 and 20 GHz, are needed to make firm conclusions about the significance of thermal emission.

From the analysis of thermal absorption properties, in the case of IC 443 (eastern rim), assuming $\Omega_S = 10^{-4}$ sr, $T_e =$ 8000–12,000 K, and $\nu_T =$ 30–50 MHz, and using Equations (8) and (9) we find $S^{\rm T}_{1\,\rm GHz} \approx$ 16–68 Jy. The flux density at 1 GHz, from the power-law fit, is around 160 Jy (Green 2009), which leads to a 10%–40% contribution of thermal emission at 1 GHz. It must be noted that the physical parameters (such as T_e and EM) of the area of thermal absorption, i.e., the eastern half of the SNR (Castelletti et al. 2011), were used here.

The integrated polarized flux density at 5 GHz for IC 443 is 2.6 $\pm$ 0.3 Jy or around 3% for the assumed integrated flux density of 84.6 ± 9.4 at 5 GHz (Gao et al. 2011). On the other hand, if we use the results from our model fit for non-thermal spectral index (0.82), and synchrotron flux density at 1 GHz (96.40 Jy), we get around 10% for mean linear polarization percentage at 1 GHz. Since the maximum polarization for synchrotron radiation is $\sim$70%, this gives a lower limit for synchrotron emission of around 15% at 1 GHz, and hence an upper limit for the thermal component of approximately 85%. Of course, one must be aware of the high uncertainties associated with α and $S^{\rm NT}_{1\,\rm GHz}$ from our model fit.

We also tried to estimate the electron density of the thermal emitting region, from our model, using Equations (14) and (15), as well as Equation (2). For $d = 1.5$ kpc (as in Castelletti et al.

[5] Scatter of residuals relative to the best-fit line (adjusted coefficient of determination).

Table 3
Fit Parameters for Our Model and a Purely Non-thermal Model for SNR 3C 391

α	$S^{\rm NT}_{1\,\rm GHz}$ (Jy)	$\frac{S^{\rm T}_{1\,\rm GHz}}{S^{\rm NT}_{1\,\rm GHz}}$	χ^2/dof	Adj. R^2
0.80 ± 0.20	21.18 ± 1.41	0.22 ± 0.11	1.34	0.99
0.56 ± 0.02	24.92 ± 0.28	...	1.57	0.99

2011), a mean angular SNR dimension of 45′ (taken from Green 2009), and for $T = 10^4$ K, we get $n_e \approx 19.5\ f^{-1/2}\,\rm cm^{-3}$. This is the (average) density, smoothed throughout the shell of the volume filling factor f. Given the crudeness of our model (and the high uncertainty associated with $S^{\rm T}_{1\,\rm GHz}$), as well as the high inhomogeneity of ISM in the vicinity of this SNR (interaction with molecular cloud), we cannot make a firm estimate of n_e and especially of the swept-up mass by the SNR. The crude estimate for the swept-up mass is $(4\pi/3)R_S^3 n_a m_{\rm H} \approx 950\,M_\odot$ for a density jump of 4 and $f = 0.25$. This is a rather high value. It must be noted that this estimate was made under the very crude assumption that the average density of ambient ISM, throughout the whole SNR's evolution, is as high as the value we estimated, for the density of the thermal emitting region. This estimate of the swept-up mass is rather the upper limit. As the classical Sedov–Taylor model is not applicable in the case of mixed-morphology SNRs, the compression could be much larger than 4 so that the ambient density could be less than $n_e/4$. The value of volume filling factor could be less than 0.25, too.

Radio recombination lines have not been detected in the direction of IC 443, but only in the direction of the adjacent H II region (Donati-Falchi & Tofani 1984). IC 443 is also detected in Hα (Keller et al. 1995). Based on the combination of the new images at 74 and 330 MHz, Castelletti et al. (2011) investigated spectral changes with position across IC 443, and related them to the spatial characteristics of the radio continuum emission and of the surrounding ISM. They concluded that thermal absorption at 74 MHz is responsible for the localized spectral index flattening observed along the eastern border of IC 443. Castelletti et al. (2011) also noted that toward the interior of IC 443 the spectrum is consistent with those expected from linear DSA, while the flatter spectrum in the southern ridge is a consequence of the strong shock/molecular cloud interaction. Electron density roughly estimated for the free–free absorbing gas is $\sim$500 cm^{-3} (Castelletti et al. 2011 and references therein). Troja et al. (2006) made a rough estimation of the total soft X-ray emitting mass of around 30 $M_\odot$. They also noted that the material emitting in the X-rays is just the outskirts of large clouds. The mean density of the X-ray emitting plasma is around 2.5 cm^{-3}, and the shock velocity corresponding to plasma temperatures of 0.3 keV is around 450 km s^{-1} (Troja et al. 2006). The SNR age is around 4 kyr (Troja et al. 2008).

4.1.2. 3C 391

From our model fit from 1 GHz to 15.5 GHz (Table 3 and Figure 7), we have 10%–25% for the contribution of thermal emission at 1 GHz. We used data from Kassim (1989), Brogan et al. (2005), and Sun et al. (2011). If we use flux densities at frequencies higher than 150 MHz (Kassim 1989; Moffett & Reynolds 1994; Brogan et al. 2005; Sun et al. 2011), from our model fit, we find that there is no significant thermal emission from 3C 391. More data, especially between 10 and 30 GHz, are needed in order to make firm conclusions about the significance of thermal emission.

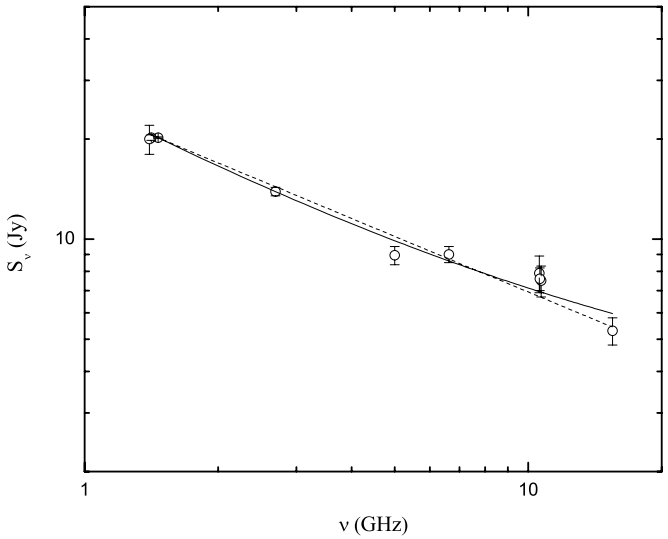

Figure 7. Integrated spectrum of SNR 3C 391. The full line represents the least-squares fit by the non-thermal plus thermal model, while the dotted line represents the fit by the purely non-thermal model. Only data on the scale of Baars et al. (1977) and frequencies higher than 1 GHz were used.

From the analysis of thermal absorption properties, in the case of 3C 391, assuming $\Omega_S = 10^{-6}$ sr, $T_e = 1000$–3000 K, and $\nu_T = 40$–150 MHz (Green 2009; Brogan et al. 2005), using Equations (8) and (9), we have $S^{\rm T}_{1\,\rm GHz} \approx 0.04$–$1.7$ Jy. The flux density at 1 GHz, from the power-law fit, is around 24 Jy (Green 2009), which leads to a 0.15%–7% contribution of thermal emission at 1 GHz.

The mean polarization fraction of 3C 391 is less than 1% at 5 GHz (Moffett & Reynolds 1994). This gives the upper limit for the thermal component of approximately 98% at 1 GHz (or lower limit for synchrotron emission of around 2% at 1 GHz).

For $d = 8$ kpc (Chen et al. 2004 and references therein), a mean angular SNR dimension of $\approx 6'$ (Green 2009), and for $T = 10^4$ K, we get $n_e \approx 46\ f^{-1/2}\,\rm cm^{-3}$ using the value for $S^{\rm T}_{1\,\rm GHz}$ from our model fit. This is the (average) density, smoothed throughout the shell of the volume filling factor f. The crude estimate for the swept-up mass is $\approx 806\,M_\odot$ for a density jump of 4 and $f = 0.25$. As we already pointed out, this value can be interpreted more as an upper limit. Also, the classical Sedov–Taylor model is not applicable in the case of mixed-morphology SNRs, so the compression could be much larger than 4 and f could be less than 0.25.

Radio recombination lines have also been observed in the direction of 3C 391. Goss et al. (1979) concluded that the thermal component responsible for the low-frequency absorption and radio recombination lines in direction of 3C 391 are due to very extended, low-density H II regions located along the line of sight to 3C 391. On the other hand, as we already mentioned, Brogan et al. (2005) found that thermal absorption could be linked to the SNR. They concluded that the free–free absorption originates from the SNR/molecular cloud shock boundaries due to ionized gas created from the passage of a J-type shock with a speed of $\sim$100 km s^{-1}. Moffett & Reynolds (1994) did not find convincing evidence for spectral index variations above their detection limit of $\Delta\alpha = 0.1$. On the other hand, Brogan et al. (2005) noted that the 330/1465 MHz spectral index map is quite uniform, but the 74/330 MHz one shows such spectral behavior that is indicative of free–free absorption at 74 MHz. Electron density of the free–free absorbing gas likely lies between 10

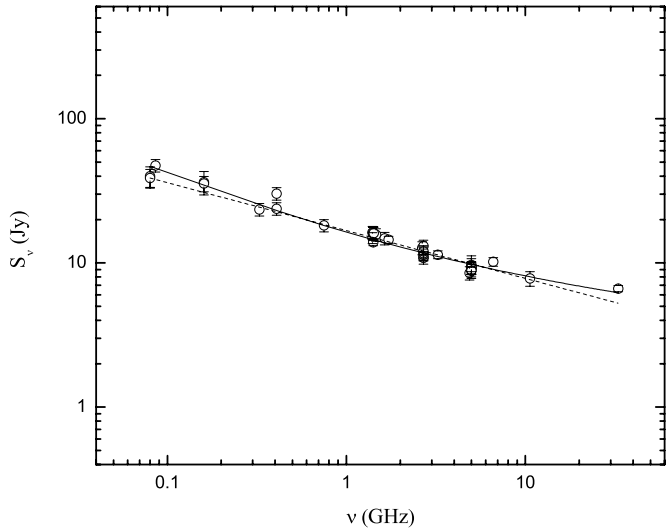

Figure 8. Integrated spectrum of SNR 3C 396. The full line represents the least-squares fit by the non-thermal plus thermal model, while the dotted line represents the fit by the purely non-thermal model.

and 10^3 cm^{-3}, with a lower range between 10 and 40 cm^{-3} favored (Brogan et al. 2005). Su & Chen (2008) pointed out that the mid-IR emission, in the direction of 3C 391, is dominated by the contribution of the shocked dust grains, which may have been partly destroyed by sputtering. Chen et al. (2004) suggested the SNR age of around 4 kyr, the mass of the X-ray emitting hot gas around 114 $f_x^{1/2}\,M_\odot$, and its mean number density of 1.9 $f_x^{-1/2}$ cm^{-3}, for the most probable SNR distance of 8 kpc, where f_x is the volume filling factor of the hot gas. Using the plasma temperature measured from the entire SNR of 0.56 keV, the velocity of the blast wave is around 680 km s^{-1} (Chen et al. 2004).

For both IC 443 and 3C 391, the errors associated with the fit parameters of our model are high. As we already mentioned, we use our simple model more for qualitative than for quantitative discussion. On the other hand, in the case of IC 443, our estimate of thermal contribution approximately agrees with that from the analysis of thermal absorption. In the case of 3C 391, the conclusions are vague as the results from our model fit and analysis of thermal absorption do not overlap. The radio spectral indices of both SNRs, from our model fit, are around 0.8, which is a rather high value. Steeper spectra ($\alpha > 0.5$) can be expected for much weaker shocks (Bell 1978a, 1978b). On the other hand, one must be aware of the parameter uncertainties from our model fit (Tables 2 and 3). The polarization observations for these SNRs also provide the possibility of significant influence of the thermal component. It must be mentioned that for the low-resolution observations, used to determine the percentage polarization, beam depolarization effects should be very important so the results must be treated with caution. Generally, tangled or disordered magnetic fields in the emitting region of the radio shell may be responsible for depolarizing the radio synchrotron radiation, as well as internal Faraday depolarization (Moffett & Reynolds 1994). We would like to stress the importance of high-frequency (>1 GHz) observations of SNRs, as well as of the reliable, high-resolution observations at low frequencies (<100 MHz) as they are necessary in order to make firmer conclusions about the existence of "radio thermally active" SNRs.

Table 4
Fit Parameters for Our Model and a Purely Non-thermal Model for SNR 3C 396

α	$S^{\rm NT}_{1\,\rm GHz}$ (Jy)	$\frac{S^{\rm T}_{1\,\rm GHz}}{S^{\rm NT}_{1\,\rm GHz}}$	χ^2/dof	Adj. R^2
0.55 ± 0.05	9.56 ± 1.14	0.71 ± 0.18	1.01	0.94
0.33 ± 0.02	16.78 ± 0.38	...	1.58	0.90

4.2. 3C 396 (G39.2−0.3)

The spectrum of 3C 396 shows a low-frequency turnover, due to thermal absorption, for which there is no firm evidence of direct connection with the SNR. On the other hand, this SNR has obvious "concave up" radio spectrum (Figure 8). Su et al. (2011) investigated the molecular environment of 3C 396 and suggested that molecular clouds at a distance of 6.2 kpc are in physical contact with this SNR. They also established a scenario for this SNR in which the SNR collides with a molecular wall in the west, with a southwestern pillar of molecular gas, and it expands in a low-density region in the east (but there also encounters a clump of backside molecular gas). In multi-wavelength morphologies, both the X-ray and radio emissions are bright in the western half and faint in the eastern half of the SNR, which is probably because of the large-scale density gradient (Su et al. 2011). Anderson & Rudnick (1993) discussed the spatial spectral index variations in this SNR. They concluded that spectral variations do not coincide with features in total intensity, although they found that the region associated with the brightest feature in the SNR (segment of the western annular enhancement, region D in Figure 4 of their work) has somewhat flatter spectral index than the SNR mean. The SNR is infrared bright, and the remnant has not been detected optically (Scaife et al. 2007 and references therein). Su et al. (2011) suggested the SNR age of around 3 kyr, mean blast shock velocity around 870 km s^{-1}, SNR radius around 7 pc, and the mass of the X-ray emitting hot gas around 70 $f_x^{1/2}\,M_\odot$, for the most probable SNR distance of 6.2 kpc, where f_x is the volume filling factor of the hot gas. They also estimated the density in the radiative shell of around 400 cm^{-3}, interclump density of around 1 cm^{-3}, and density in the clump of around 10^4 cm^{-3}. The X-ray bright synchrotron pulsar wind nebula (PWN), surrounding a yet undetected pulsar, is located in the center of the SNR (Olbert et al. 2003).

4.2.1. The Results of Our Model Fit

We used the data points from Patnaik et al. (1990), Scaife et al. (2007), and Sun et al. (2011) between 80 MHz and 33 GHz. The cataloged flux densities for SNR 3C 396 are contaminated by the nearby steep-spectrum pulsar, PSR 1900+0.5, below 30 MHz (Scaife et al. 2007) or 100 MHz (Patnaik et al. 1990). Olbert et al. (2003) emphasized that the PWN, near the center of the SNR, contributes $\leqslant 1/25$ of the total radio flux density at 1.4 GHz. The parameters of our model and a purely non-thermal model fit are shown in Table 4. In Figure 8, the full line represents a fit to the SNR 3C 396 data by the non-thermal plus thermal model, while the dotted line represents fit by a purely non-thermal model. We have compared our model with the (simple) power-law model. From the χ^2 statistics we conclude that the non-thermal plus thermal model gives a much better fit than a pure non-thermal model for SNR 3C 396. From our model, the thermal emission in the case of SNR 3C 396 contributes 35%–47% of the total flux density at 1 GHz. Excluding the

points below 100 MHz does not change our results significantly. More data, especially between 10 and 30 GHz, are needed to make firm conclusions about the significance of thermal emission.

4.2.2. Discussion on a Low-frequency Turnover

The low-frequency spectrum of SNR 3C 396 (see Figure 10 in Patnaik et al. 1990) shows a turnover below 80–100 MHz (Anderson & Rudnick 1993). For spectral turnover due to thermal absorption around 40–80 MHz, the electron temperature would be order of $T_e \approx (1\text{–}6) \times 10^4$ K (using Equation (8)) for our model. In that case, the emission measure is EM $\approx 10^{4-5}$ cm^{-6} pc. On the other hand, our results are not consistent with the work of Anantharamaiah (1985), who gave an upper limit on the emission measure of 280 cm^{-6} pc and electron temperature of 5000 K for the gas, which leads to $\nu_T \approx 20$ MHz and thermal contribution of 0.8% at 1 GHz. If we keep $T_e =$ 5000 K but put $\nu_T =$ 40–80 MHz we have EM $\approx 10^3$ cm^{-6} pc and not significantly higher thermal contribution of ≈0.9% at 1 GHz. Anantharamaiah (1985) also noted that the upper limits implied by the pulsar dispersion measure (Table 4 in the mentioned work) are not rigorous due to the assumptions made. Hewitt et al. (2009) pointed out, from the *Spitzer* IRS observation analysis, that along the western shell, the inner [Fe II]-line filament and the outer H_2-line one are found to be spatially separated. Their results are in a good agreement with the near-IR observations of Lee et al. (2009). Hewitt et al. (2009) used observations of strong ionic lines, and found $n_e = 270$ cm^{-3}, $T_e = 2.3 \times 10^4$ K from the [Fe II] 7.9/5.35 μm, and 17.9/26 μm ratios. On the other hand, Lee et al. (2009), using the Wide-Field Infrared Camera on board the Palomar 5 m Hale telescope, found an upper limit of <2000 cm^{-3} for the electron number density of the [Fe II] 1.64 μm emission gas for an assumed temperature of 5000 K. The increased abundance of gas phase iron by shock-induced sputtering of the dust grains and/or the creation of an extensive partially ionized zone by shock heating can substantially enhance the [Fe II] emission and also implies that most of the dust has been destroyed (Lee et al. 2009 and references therein). Given the very complex nature of this remnant (high-density gradients, interaction with molecular clouds), the shape of the integrated radio spectrum from 10 to 100 MHz, as well as its multi-wavelength properties, the presence of thermal emission for 3C 396 is uncertain. We point out that spatially resolved low-frequency radio observations are needed to make firmer conclusions. We propose, for a future work, the observations of SNR 3C 396, with one telescope, VLA,[6] over a wide frequency range. That would also include obtaining the high-resolution radio images at 74 and 330 MHz for a sensitive, spatially resolved, spectral analysis of the radio emission at long wavelengths.

The bright 24 μm mid-IR emission, in the direction of 3C 396, may chiefly come from dust grains and even from the ionic and molecular species in the shocked gas produced when the western molecular wall was hit by the SNR blast wave (Su et al. 2011 and references therein). Scaife et al. (2007) have assessed the possibility of spinning dust emission at 33 GHz toward the SNR 3C 396. They also concluded that further measurements are required in the range 10–20 GHz in order to confirm that. These measurements will also help determine if there is significant thermal emission from 3C 396.

[6] The Very Large Array of the National Radio Astronomy Observatory is a facility of the National Science Foundation operated under cooperative agreement by Associated Universities, Inc.

4.2.3. Linear Polarization Measurements

From a linear polarization analysis at 5 GHz, Patnaik et al. (1990) state that the polarization percentages toward the eastern edge of the SNR reach about 50%. On the other hand, on the SW and NW shell structure, the polarization is typically 6%–7%. The central polarized island is about 10% polarized, while the rest of the interior has a percentage polarization of ⩽3% (Patnaik et al. 1990). Sun et al. (2011) found an integrated polarized flux density at 5 GHz 240 ± 15 mJy. The average percentage polarization is 3% if we assume the integrated flux density at 5 GHz of 8.84 ± 0.53 Jy from their work. On the other hand, if we use the results from our model for non-thermal spectral index (0.55) and synchrotron flux density at 1 GHz (9.56 Jy), we get around 6% for mean linear polarization percentage at 1 GHz. This gives an upper limit for the thermal component of approximately 91% at 1 GHz (or lower limit for synchrotron emission of around 9% at 1 GHz). Of course, as we already noted, one must be aware of the uncertainties associated with α and $S^{\rm NT}_{1\,\rm GHz}$ from our model fit.

4.2.4. The Density and Swept-up Mass Estimation

For $d = 6.2$ kpc (as in Su et al. 2011), a mean angular SNR dimension of ≈7′ (Green 2009), and for $T = 10^4$ K we get $n_e \approx 50\ f^{-1/2}$ cm^{-3} using the value for $S^{\rm T}_{1\,\rm GHz}$ from our model fit. This is the (average) density, smoothed throughout the shell of the volume filling factor f. Given the crudeness of our model, as well as high inhomogeneity of ISM in the vicinity of this SNR (interaction with molecular cloud), we cannot make a firm estimate of n_e and especially of the swept-up mass. The crude estimate of the swept-up mass is ≈650 $M_\odot$ for a density jump of 4 and $f = 0.25$. This value can be interpreted more as an upper limit. Such an estimate was made by the very crude assumption that the average density of ambient ISM, throughout the whole SNR's evolution, is as high as the value we estimated, for the density of the thermal emitting region.

5. CONCLUSIONS

In this work, we investigated the possibility of significant production of thermal bremsstrahlung radiation at radio continuum frequencies intrinsic to some Galactic SNRs.

1. There are several possible tracers of significant radio thermal bremsstrahlung radiation from SNRs, such as: a "concave up" radio spectrum (flattening at higher frequencies), thermal absorption at lower frequencies intrinsic to the SNR, and flat spectral indices (radio spectral index variations) associated with high-density regions which do not show high linear polarization.
2. The main targets for investigation of the presence of significant radio thermal emission are SNRs expanding in high density as well as in inhomogeneous environments such as those interacting with molecular clouds. The evolution as well as the radiation from such SNRs is more complex than usually considered in models such as for Sedov–Taylor evolution.
3. In this work, we discussed the radio continuum properties of three SNRs that are good candidates for testing our hypothesis on significant thermal emission. In the case of the SNRs IC 443 and 3C 391, thermal absorption, linked to the SNRs, was previously detected. For the IC 443, the contribution of the thermal emission (3%–57% at 1 GHz) approximately agrees with the estimate obtained from

low-frequency thermal absorption (10%–40% at 1 GHz). For SNR 3C 391 the results of our model fit (10%–25% at 1 GHz) have higher values than those from the analysis of thermal absorption (0.15%–7% at 1 GHz). In the case of the SNR 3C 396, we suggest that thermal absorption could be linked to the SNR and propose that the thermal emission (<47% at 1 GHz from our model fit) could be significant enough to shape the radio continuum spectrum at high frequencies. The polarization observations for these SNRs also allow the presence of a significant thermal component.

4. The small number of data points (with acceptable associated errors) and the dispersion of flux densities at the same frequencies prevent us from firm quantitative analysis. Reliable observations at low frequencies (<100 MHz), as well as more data at radio frequencies higher than 1 GHz, are necessary in order to make stronger conclusions about the existence of "radio thermally active" SNRs.
5. We propose, for a future work, a systematic survey of candidate "radio thermally active" SNRs, especially SNR 3C 396, with one telescope (the eVLA) over a wide frequency range. That would also include obtaining high-resolution radio images at 74 and 330 MHz for a sensitive, spatially resolved, spectral analysis of the radio emission at long wavelengths.
6. The analysis of possible thermal bremsstrahlung radio emission inherent to some Galactic SNRs could be a very important tool for the estimation of density in which Galactic or extragalactic SNRs are embedded.

We thank the anonymous referee for useful suggestions which substantially improved this paper. This work is part of the projects 176005 "Emission nebulae: structure and evolution" supported by the Ministry of Education and Science of Serbia. D.A.L. acknowledges support from the Natural Sciences and Engineering Research Council of Canada.

REFERENCES

Allen, G. E., Houck, J. C., & Sturner, S. J. 2008, ApJ, 683, 773
Altenhoff, W. J., Mezger, P. G., Wendker, H., & Westerhout, G. 1960, Veröff. Sternwärte Bonn, 59, 48
Anantharamaiah, K. R. 1985, J. Astrophys. Astron., 6, 203
Anderson, M. C., & Rudnick, L. 1993, ApJ, 408, 514
Baars, J. W. M., Genzel, R., Paulinu-Toth, I. I. K., & Witzel, A. 1977, A&A, 61, 99B
Bandiera, R., & Petruk, O. 2004, A&A, 419, 419
Bell, A. R. 1978a, MNRAS, 182, 147
Bell, A. R. 1978b, MNRAS, 182, 443
Bell, A. R., Schure, K. M., & Reville, B. 2011, MNRAS, 418, 1208
Berezhko, E. G., & Völk, H. J. 2004, A&A, 427, 525
Brogan, C. L., Lazio, T. J., Kassim, N. E., & Dyer, K. K. 2005, AJ, 130, 148
Castelletti, G., Dubner, G., Clarke, G. T., & Kassim, N. E. 2011, A&A, 534, 21
Chen, Y., Su, Y., Slane, P. O., & Wang, Q. D. 2004, ApJ, 616, 885
Chomiuk, L., & Wilcots, E. M. 2009, ApJ, 703, 370
Cooray, A., & Furlanetto, S. R. 2004, ApJ, 606, L5
Donati-Falchi, A., & Tofani, G. 1984, A&A, 140, 395
Drury, L. O'C., Aharonian, F. A., Malyshev, D., & Gabici, S. 2009, A&A, 496, 1D
Duric, N., Bourneuf, E., & Gregory, P. C. 1988, AJ, 96, 81
Gao, X. Y., Han, J. L., Reich, W., et al. 2011, A&A, 529, 159
Gayet, R. 1970, A&A, 9, 312
Goss, W. M., Skellern, D. J., Watkinson, A., & Shaver, P. A. 1979, A&A, 78, 75
Green, D. A. 2009, A Catalogue of Galactic Supernova Remnants (2009 March version), Astrophysics Group, Cavendish Laboratory, Cambridge, UK (http://www.mrao.cam.ac.uk/surveys/snrs/)
Hewitt, J. W., Rho, J., Andersen, M., & Reach, W. T. 2009, ApJ, 694, 1266
Hewitt, J. W., & Yusef-Zadeh, F. 2006, BAAS, 38, 122
Kassim, N. E. 1989, ApJ, 71, 799
Keller, L. D., Jaffe, D. T., Pak, S., Luhmal, P. L., & Claver, C. F. 1995, RevMexAA Conf. Ser., 3, 251
Leahy, D. A. 2006, ApJ, 647, 1125
Leahy, D. A., & Roger, R. S. 1998, ApJ, 505, 784
Leahy, D. A., & Tian, W. W. 2006, A&A, 451, 251
Leahy, D. A., Xizehn, Z., Xinji, W., & Jiale, L. 1998, A&A, 339, 601
Lee, H.-G., Moon, D.-S., Koo, B.-C., Lee, J.-J., & Matthews, K. 2009, ApJ, 691, 1042
McKee, C. F., & Ostriker, J. P. 1977, ApJ, 218, 148
Moffett, D. A., & Reynolds, S. P. 1994, ApJ, 425, 668
Olbert, C., Keohane, J. W., Arnaud, K. A., et al. 2003, ApJ, 592, L45
Onić, D., & Urošević, D. 2008, Serb. Astron. J., 177, 67
Ostrowski, M. 1999, A&A, 345, 256
Patnaik, A. R., Hunt, G. C., Salter, C. J., Shaver, P. A., & Velusamy, T. 1990, A&A, 232, 467
Petruk, O. 2005, J. Phys. Stud., 9, 364
Pynzar', A. V., & Shishiv, V. I. 2007, Astron. Rep., 51, 1
Reynolds, S. P. 2008, ARA&A, 46, 89
Reynolds, S. P. 2011, Ap&SS, 336, 257
Reynolds, S. P., & Ellison, D. C. 1992, ApJ, 399, L75
Rho, J., & Petre, R. 1998, ApJ, 503, L167
Scaife, A., Green, D. A., Battye, R. A., et al. 2007, MNRAS, 377, L69
Schlickeiser, R., & Fürst, E. 1989, A&A, 219, 192
Stupar, M., & Parker, Q. A. 2011, MNRAS, 414, 2282S
Su, Y., & Chen, Y. 2008, Adv. Space Res., 41, 401
Su, Y., Chen, Y., Koo, B.-C., et al. 2011, ApJ, 727, 43
Sun, X. H., Reich, P., Reich, W., et al. 2011, A&A, 536A, 83S
Tian, W. W., & Leahy, D. A. 2005, A&A, 436, 187
Tilley, D. A., Balsara, D. S., & Howk, J. C. 2006, MNRAS, 371, 1106
Troja, E., Bocchino, F., Miceli, M., & Reale, F. 2008, A&A, 485, 777
Troja, E., Bocchino, F., & Reale, F. 2006, ApJ, 649, 258
Truelove, J. K., & McKee, C. F. 1999, ApJS, 120, 299
Uchiyama, Y., Roger, D., Blandford, R. D., et al. 2010, ApJ, 723, L122
Urošević, D., & Pannuti, T. G. 2005, Astropart. Phys., 23, 577
Urošević, D., Pannuti, T. G., & Leahy, D. 2007, ApJ, 655, L41
Vink, J. 2012, A&AR, 20, 49
Vink, J., Tamazaki, R., Helder, E. A., & Schure, K. M. 2010, ApJ, 722, 1727
Yamaguchi, H., Ozawa, M., & Ohnishi, T. 2012, Adv. Space Res., 49, 451
Yamauchi, S., Koyama, K., Tomida, H., Yokogawa, J., & Tamura, K. 1999, PASJ, 51, 13